Energy 116 (2016) 1039–1050

Contents lists available at ScienceDirect

Energy

journal homepage: www.elsevier.com/locate/energy

Experimental study of a parabolic trough solar collector with flat bar-and-plate absorber during direct steam generation

Matteo Bortolato [a, b], Simone Dugaria [a], Davide Del Col [a, *]

[a] Department of Industrial Engineering (DII), University of Padova, Via Venezia 1, 35131, Padova, Italy
[b] Interdepartmental Centre "Giorgio Levi Cases" for Energy Economics and Technology, University of Padova, Via Francesco Marzolo 9, 35131, Padova, Italy

ARTICLE INFO

Article history:
Received 6 July 2016
Received in revised form
30 September 2016
Accepted 7 October 2016
Available online 24 October 2016

Keywords:
Solar energy
Solar process heat
Parabolic trough collectors
Enhanced receiver
Experimental tests
Direct steam generation

ABSTRACT

The present work aims at investigating an innovative flat aluminum absorber for process heat and direct steam generation in small linear solar concentrating collectors. After defining its optimal width through a Monte Carlo ray-tracing analysis, this absorber has been manufactured with the bar-and-plate technology, including an internal offset strip turbulator in the channel. This technology is cost-effective and extremely flexible, allowing to easily adapt the geometry of the absorber to different reflecting optics configurations. It has been mounted on an asymmetrical parabolic trough concentrator to form a solar collector with a concentration ratio of 42, which has been experimentally investigated. In particular, a new test procedure is presented, applied and validated to characterize the thermal performance of the collector during steam generation. The results show that a promising overall thermal efficiency of 64% at 0.160 K m^2 W^{-1} can be achieved with negligible pressure drop.

1. Introduction

The conversion of solar energy into heat in the medium temperature range (between 80 °C and 250 °C) has recently encountered a renewed interest. After concluding tests in several pilot plants, solar collectors manufacturers offer some proven solutions on the market. On the other hand, research institutions are investigating on several topics, including the improvement of the global system control, the cost-effectiveness, the building integration and new solutions to overcome the technical issues encountered in practice. There are several environmental, political and economic reasons that justify this interest. Medium temperature solar collectors are very suitable for many commercial and industrial applications, such as the industrial process heat, the solar cooling and the desalination of the seawater. As these devices exploit a renewable energy source, they may contribute to the reduction of the energy supply from fossil fuels and greenhouse gases emissions.

According to the IEA statistics of 2013 [1], industry represents around 30% of the total final consumption of energy worldwide. Electricity accounts for the 26% out of the final energy use for industry, while the rest is the industrial heat demand. Market potential analysis performed in 2006 on medium temperature solar collectors [2] showed more or less the same share for the industrial heat demand and pointed out that, as a general tendency, about 50% of the industrial process heat demand is located at temperatures up to 250 °C. Vannoni et al. [3] highlighted several industrial key sectors such as food, textile, transport equipment, chemical, metal and plastic treatment, that present 60% of the thermal energy demand at a temperature level that encourages the use of solar process heat.

Moreover, the air-conditioning and refrigeration systems powered by solar thermal collectors are becoming an efficient and, in some cases, competitive alternatives to the conventional systems to meet the increasing cooling demand of big buildings and the refrigeration requirements in food processing and pharmaceutical products conservation. The most attractive prospect is the achievement of a temperature level high enough (150°C-200 °C) to couple the solar collectors with double effect absorption chillers [4]. It is worth to remember that in most industrialized countries, the air-conditioning demand shifts the yearly peak of electrical energy consumption in summer and may cause serious problems to the stability of the electrical grid.

Solar desalination of the seawater might become one of the principal means to assure the access to drinking and safe water to

* Corresponding author.
E-mail address: davide.delcol@unipd.it (D. Del Col).

http://dx.doi.org/10.1016/j.energy.2016.10.021
0360-5442/

Nomenclature

A	area, m^2
c	isobaric specific heat capacity, J kg^{-1} K^{-1}
c_1	heat loss coefficient, W m^{-2} K^{-1}
c_2	temperature dependence of the heat loss coefficient, W m^{-2} K^{-2}
c_3	wind speed dependence of the heat loss coefficient, J m^{-3} K^{-1}
c_4	sky temperature dependence of the heat loss coefficient
c_5	effective thermal capacity, J m^{-2} K^{-1}
c_6	wind speed dependence in the zero loss coefficient, s m^{-1}
DNI	direct normal irradiance, W m^{-2}
E_L	long wave irradiance, W m^{-2}
G	hemispherical solar irradiance, W m^{-2}
G_b	direct solar irradiance, W m^{-2}
G_d	diffuse solar irradiance, W m^{-2}
h	specific enthalpy, J kg^{-1}
h_{LV}	specific latent heat of vaporization, J kg^{-1}
K	incidence angle modifier
$\dot{m}$	mass flow rate, kg s^{-1}
p	absolute pressure, bar
$\dot{q}$	heat transfer rate, W
T	temperature, K
t	temperature, °C
t_m^*	reduced temperature difference, K m^2 W^{-1}
u	wind speed, m s^{-1}
x	thermodynamic vapor quality
X, Y, Z	rectangular coordinates, mm

Greek letters

γ	intercept factor
η	efficiency
σ_{SB}	Stefan-Boltzmann constant, W m^{-2} K^{-4}
τ	time, s
τ_C	collector time constant, s
Φ	concentrated flux, W m^{-2}

Subscripts

0	optical
abs	absorber
amb	ambient air
ap	aperture
b	beam (or direct) irradiance
d	diffuse irradiance
eq	equivalent
HE	heat exchanger
I	primary loop
II	secondary loop
in	inlet
L	saturated liquid
m	mean
mir	mirrors
out	outlet
R	receiver
th	thermal

everybody, given that the highest solar energy availability and the troubles of clean water supply pertain to the same regions.

1.1. Literature review on thermal receivers for linear solar concentrating collectors

Many researchers agree that, from a technical point of view, the parabolic trough collectors are the best proven and reliable solar technology for the production of heat in the medium temperature range, mainly thanks to the experience and the know-how gained in large commercial concentrated solar power (CSP) plants. Fernandez-Garcia et al. [5] and Zarza [6] presented an overview on the components, efficiency and applications of these concentrating solar collectors, including commercial plants and new prototypes. Linear Fresnel collectors also represent a viable alternative for the conversion of the solar energy into heat in the medium temperature range.

The present work focuses on the receiver, that is the heart of any linear solar concentrating collector. In parabolic trough collectors, the receiver is generally formed by an inner steel tube provided with a selective coating on its external surface that acts as surface absorber and a glass envelope to reduce thermal losses. On the other side, linear Fresnel collectors admit many configurations of receivers [7,8] and the following categories can be distinguished for a general classification:

- non evacuated single tube and secondary optics,
- evacuated single tube and secondary optics,
- inverted trapezoidal cavity receiver [9,10].

In these collectors, the solar concentrated flux incident on the absorber element of the receiver is a function of direct normal irradiance, geometrical concentration ratio, optical properties of the materials and total optical errors of the system. In typical configurations, the distribution of the concentrated solar flux on the surface of the absorber is strongly non uniform [11,12]. This can lead to a temperature gradient along the cross section of the absorber which is associated to differential thermal expansions. The resulting thermal stresses may have serious effects, especially in some particular working conditions. As reported by Wang et al. [13], the temperature difference on the cross section of the absorber should be not too high to allow a safety and reliable operation. Khanna and coworkers [11,14,15] derived explicit expressions to calculate circumferential and axial distribution of the concentrated flux, temperature distribution, radial, circumferential and axial distribution of normal stresses and strains on the absorber of a parabolic trough receiver and the corresponding deflection in its central axis. The expression for the realistic distribution of the concentrated flux is achieved by implementing Gaussian sun shape and optical errors in a Monte Carlo ray tracing tool. The use of these tools is of great importance to obtain reliable results when performing numerical investigations on the receiver of a concentrating collector. The presented expressions are useful to find the appropriate dimensions of the parabolic trough collector, to design the support brackets, to evaluate the appropriate gap between the glass envelope and the absorber tube in a typical receiver and to define the optimal mass flow rate. In common practice, a high mass flow rate is pumped in order to achieve a turbulent flow condition inside the absorber tube but this may not always be the optimal strategy.

Circumferential and axial thermal gradients on the absorber tube included in a glass envelope represent a major concern in liquid heating concentrating collectors working with low mass flow rates. In fact, in these cases, due to the low heat transfer coefficients, a bending of the tube can occur and the possible breakage of the glass envelope jeopardizes the thermal efficiency. Furthermore, the deviation of the receiver from the focal line may also reduce the intercept factor and consequently the optical efficiency. This situation is worse when low conductivity thermal oil is used as heat transfer fluid: the peak temperature not only may damage the selective coating but also may provoke the chemical degradation of the oil.

In the open literature, many passive techniques have been proposed for receivers in parabolic trough collectors to reduce circumferential temperature gradient, peak temperature, exergy losses, to enhance the internal heat transfer and to increase the overall collector efficiency. Passive heat transfer enhancement generally involves three mechanisms to promote the turbulence of the flow: decreasing thermal layer, increasing the flow disturbance and increasing the velocity gradient near solid walls. Most of the available works are numerical investigations comparing conventional and enhanced receivers in parabolic troughs for CSP plants. Some numerical works assuming a realistic non uniform flux on the absorber tube, derived by a Monte Carlo ray tracing method, are reviewed below. In the work by Muñoz and Abanades [16], the effect on pressure drop, thermal losses, thermo-mechanical stress and thermal fatigue of a set of internal helically finned absorber tubes with different number of fins and helix angles has been analyzed by computational fluid dynamics (CFD) tools. Cheng et al. [17] carried out a numerical computation of several receivers with unilateral longitudinal vortex generators, located on the side of the absorber tube where the solar irradiance is concentrated. As compared to the smooth absorber, the different geometries of enhanced internal surfaces exhibit better heat transfer performance in a wide range of working conditions. Gadirijafarbeigloo et al. [18] presented numerical simulations concerning the use of typical twisted tape inserts and innovative perforated louvered twisted tape inserts inside the absorber tube and showed that the latter allow higher thermal performance especially at low Reynolds numbers. Helical screw-tape inserts in absorber tubes have been suggested by Song et al. [19] as an improvement of common twisted tape inserts to level out the temperature distribution specifying that experiments are required to verify their performance. Mwasigye et al. [20,21] numerically optimized the geometry of perforated plate inserts centrally placed inside an absorber tube and fixed to a connecting rod. The optimization of orientation, spacing and diameter of the plates takes into account not only heat transfer enhancement and fluid friction but also the entropy generation in a wide range of operating conditions.

One of the few experimental works available on thermal receivers for heat transfer enhancement has been presented by Reddy et al. [22]. They investigated the performance of six different receiver configurations in a 3 m long parabolic trough collector with an aperture width of 2.5 m. The external diameter of all the absorbers is of 60 mm. The investigated configurations include: conventional receivers with and without glass envelope and enhanced receivers with bottom porous discs, U-shaped bottom porous discs, inclined bottom porous discs and alternative porous discs. Results showed that the use of inserts lead to lower thermal gradients between the receiver wall surface and fluid and across the receiver cross section. The best performance has been achieved using alternative porous discs and the relevant increase in pumping power is negligible. The authors proposed this solution both for solar power and process heat applications.

1.2. Receivers for steam generation in linear solar concentrating collectors

The non uniform distribution of the concentrated flux on the absorber must be taken into account above all when direct steam generation is performed. In fact, the phase change can be associated with a large variation of the heat transfer coefficient along the cross section of the absorber with changing vapor quality when a stratified flow regime is established. As a consequence, a significant angular thermal gradient appears. Nevertheless, in the medium temperature range, direct steam generation is very attractive. In these applications, the working pressure is not very high and a cost reduction of the energy produced from the solar source and an increase in the efficiency of the system can be achieved. In fact, as compared to the use of liquid water, the phase change reduces the mass flow rate through the pumping system. Moreover, the heat exchanger between the solar collectors and the thermal user may be removed. With respect to the use of the thermal oil, direct steam generation allows to eliminate some auxiliary equipments and reduces the environmental impact of the system.

There are essentially two strategies to attain a strong reduction of the thermal gradient in direct steam generation [23]. The first one is to avoid working under stratified regime, setting a mass flow rate high enough to operate under annular flow pattern. This strategy involves the calculation of a lower limit for the mass flow rate that depends on the working conditions and on the geometry of the absorber and it is generally employed in the rare CSP plants working with steam. The second one concerns either the adoption of a high thermal conductivity material in the manufacturing of the absorber tube or the integration of enhanced heat transfer systems. This approach entails no lower limit of the operating mass flow rate and gives higher flexibility to the plant. In fact, it can work even under lower solar radiation and for a higher number of hours per day. This is of great interest especially in small linear concentrating collectors for medium temperature applications; nevertheless, most of the relevant works available in the open literature focus on big parabolic troughs for solar power. Almanza et al. [24,25] investigated mild steel and copper absorbers behavior under two phase stratified flow tests in a parabolic trough solar collector. When using the steel pipe, at around 160 °C wall temperature, a maximum deflection of 6.5 cm has been observed causing the breaking of the glass envelope. In this case, the maximum circumferential temperature difference was around 60 °C. Under the same test conditions, using a copper pipe, a bend of 2 mm has been observed and a maximum temperature difference of 10 °C has been measured. The authors highlighted that thermal cycles at high temperature may cause copper annealing. On the basis of these results, Flores and Almanza [26] compared the thermal behavior of a bimetallic copper-steel receiver for direct steam generation in parabolic trough solar collectors. Experiments have been performed in transient conditions, simulating the presence of clouds. The results prove that the high thermal conductivity of the internal copper layer contributes to uniform the wall temperature of the receiver while the external steel layer improves the mechanical resistance. At a mass flow rate of 150 kg h^{-1} and at a wall temperature around 200 °C, the deformation reaches 70 mm in steel receiver and 18 mm in the bimetallic receiver. Moreover, the thermal behavior of the bimetallic receiver resulted to be slightly affected by the variation of the incidence angle of the solar beam irradiance. A numerical CFD simulation has been carried out by Aldali et al. [27] to assess the use of three types of tubes with different internal helical fins and an aluminum pipe without any fins as absorbers in a parabolic trough solar collector for direct steam generation under realistic heat flux distribution around the tube. The results show that the presence of fins improves the

thermal distribution, but the smaller the pitch of the fins, the higher the pressure drop. The aluminum pipe has proved to be the best solution in minimizing the thermal stress so the thermal conductivity of the absorber tube may play an important role in reducing the circumferential temperature gradient. Rojas et al. [23] presented a methodology to assess the applicability of porous coating and etched microgrooves as capillary systems on the internal wall of the surface absorber tube of a parabolic trough solar concentrating collector for direct steam generation.

The present work investigates an innovative aluminum flat absorber for medium temperature linear concentrating solar collectors. The absorber has been manufactured with bar-and-plate technology and provided with an internal turbulator. According to the cited studies in the literature, the combined use of a high thermal conductivity material and of passive heat transfer enhancement devices should make the direct steam generation easier to control and less critical. The performance of the new absorber is experimentally assessed in an asymmetrical parabolic trough collector under single phase and two phase flow regimes. For the latter case, a new test method is proposed and validated.

2. The present solar collector prototype

2.1. Geometry of concentrator and receiver

The linear solar concentrating collector considered in this work has been installed in the Solar Energy Conversion Lab of the Industrial Engineering Department, at the University of Padua. It includes a prototype of an asymmetrical small parabolic trough concentrator (Fig. 1) and an innovative receiver. The present concentrator can be seen as half of a more common symmetric parabolic trough for CSP applications. Its cross section is a segment of a parabola that extends from the vertex to the mirror rim. More precisely, the lower rim of the reflective optics is on the parabolic profile at 35 mm from the vertex line, to allow the arrangement of the receiver without any shading. The present geometry exhibits an aperture width of 2.91 m, a rim angle of 78.7° and a focal length of 1.81 m. The length of the trough is equal to 2.4 m and the aperture area is equal to 6.984 m^2. The concentrator is made up by four back silvered glass facets available on the market, which have a nominal solar reflectivity of 96%, as provided by the manufacturer. The prototype is supplied with a two-axes solar tracking system to have the direct irradiance normal to the aperture area without any cosine loss while working. The motion is governed by a solar algorithm when approaching the sun and by a sun sensor when achieving the best receiver alignment. The particular geometry and the tracking system has been adopted for experimental research purposes to facilitate the arrangement the sensors and the control of the device. Furthermore, this parabolic trough concentrator is suitable to be coupled with a receiver displaying a flat geometry absorber rather than a tubular receiver. In the present concentrator, the absorber has been designed so that its front surface is 45° tilted with respect to the aperture plane. This solution derives from a compromise between the needs to minimize the incidence angle of the concentrated beams and to make simple the positioning of the receiver.

Fig. 1. Prototype of the asymmetrical parabolic trough linear solar concentrator used in the present experimental study.

The dimensions of the absorber front surface have been defined by developing an optical model of the present asymmetrical concentrator using SolTrace [28] as Monte Carlo ray-tracing (MCRT) tool. In the model, the reflectivity of the mirror facets, the sun shape and the total optical error have been taken into account and the rays coming from the sun have been assumed normal to the aperture area, as provided by the two-axes tracking system. The sun shape profiles implemented in SolTrace refer to the work by Neumann et al. [29], in which the average solar brightness profile has been defined at different values of circumsolar ratio. In particular, the sun shape CSR0 describing the most probable terrestrial sun brightness profile on a clear sky has been considered for the present design.

According to the CSR0 profile, the circumsolar radiation represents up to 4% of the total energy contained in the solar disk plus aureole. A Gaussian distribution has been used to model the total optical error, including tracking, mirror slope, reflecting surface, receiver alignment and position errors. In the numerical analysis, the total optical error is applied to the parabolic mirrors. A typical value for the total optical error of 5 mrad and a range of absorber widths from 40 mm to 100 mm have been considered. During the numerical study, the desired number of rays intersections has been set equal to $3 \cdot 10^6$: the use of more rays intersections has a negligible effect on the estimation of the optical performance parameters, while implying a much higher computational effort. The present MCRT analysis allows to calculate the intercept factor that is the ratio of the radiative flux reaching the absorber to the one reflected by the mirrors (Eq. (1)).

$$\gamma = \frac{\Phi_{abs}}{\Phi_{mir}} \tag{1}$$

Fig. 2 depicts the calculated intercept factor as a function of the absorber width. Because of the model adopted to represent the total optical error, when increasing the width of the absorber, the numerical predictions of the intercept factor tend asymptotically to a value between 99% and 100%, but this has a minor effect on the design of the receiver. It is clear to see that the intercept factor does not increase significantly for widths higher than 70 mm. Furthermore, the bigger the absorber width, the higher the thermal losses towards the external surroundings. As a consequence, a width of

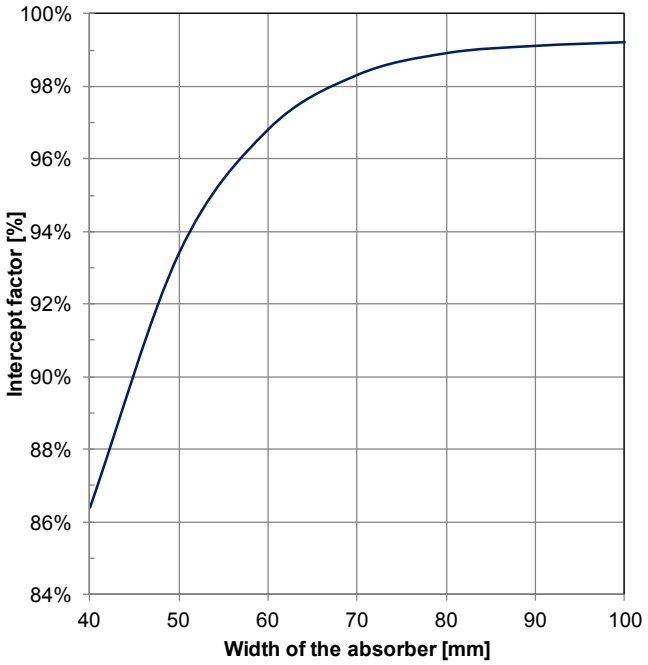

Fig. 2. Intercept factor at different widths of the absorber. Values have been calculated using SolTrace and considering a total optical error of 5 mrad.

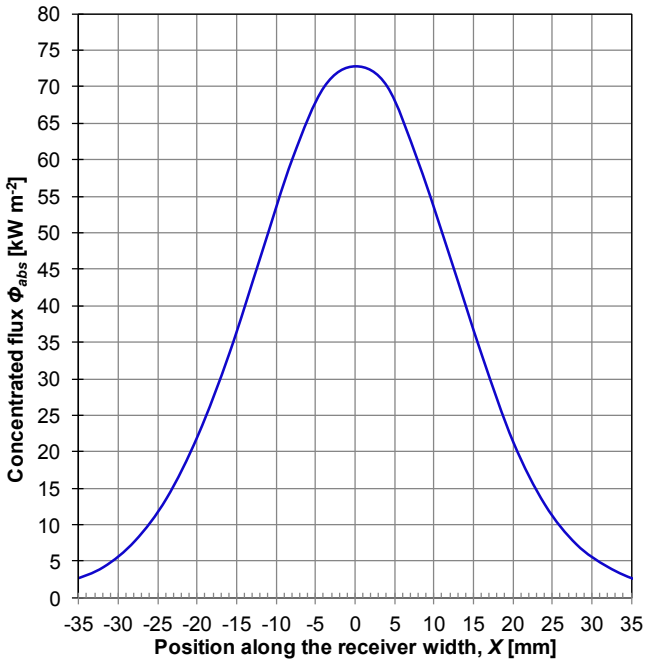

Fig. 3. Average concentrated flux distribution Φ_{abs} along the established absorber width (70 mm) evaluated using SolTrace and considering a total optical error of 5 mrad.

70 mm has been adopted for the absorber, thus the geometrical concentration ratio is equal to 42. The length of the receiver is equal to 1.2 m, which is half of the total trough length. The absorber has been arranged so that it receives the concentrated solar flux from a single row of back silvered glass facets. Due to the two-axes tracking system, the second mirror row does not influence the performance of the present absorber, thus, the thermal efficiency can be computed considering a trough length of 1.2 m. A modular configuration can be considered for the system, which means that, for the physical application, more receivers can be installed in parallel. For this reason, only one 1.2 m long receiver has been studied here.

The optical model provides the solar flux map on the front surface of the absorber. Starting from this map, the mean flux distribution profile at a direct normal irradiance of 850 W m^{-2} (Fig. 3) has been calculated as the average of the flux distributions along the front surface of the absorber. In this way, the deviations among the flux profiles along the absorber length due to the ray-tracing technique here adopted can be neglected. In the calculation, the width of the absorber has been discretized into 25 bins, while 40 bins have been set for the absorber's length. A finer resolution does not affect the definition of the average flux distribution profile. The distribution of the concentrated flux is strongly non uniform and exhibits a maximum at the position 0, which corresponds to the focal line. Considering this highly non uniform heat flux profile, the use of a heat spreader is recommended to reduce the thermal load on the central line of the absorber and to use more effectively the heat transfer area on the working fluid side. It can consist of a front plate with a thickness of 5–10 mm made of a high thermal conductivity material.

The bar-and-plate technology is suitable to manufacture an absorber with the features derived from the MCRT analysis. In fact, it allows to create a rectangular channel made of aluminum with high mechanical stiffness, including a heat spreader on the front surface reached by the non uniform concentrated solar flux. The heat spreader here is made of a thick aluminum plate on the front face. Furthermore, it gives the possibility to include a turbulator inside the channel, which enhances the heat transfer and may play a pivotal role during direct steam generation. The presence of the turbulator entails an uniform distribution of the mass flow rate on the absorber cross section, hence stagnation points leading to hot spots can be avoided. Furthermore, the hydraulic diameter is reduced and the occurrence of a stratified flow regime is limited. Finally, the turbulator helps to increase the nucleation sites and favors the trigger of the vaporization.

Given the above, throughout the length of the present absorber, there is an offset strip turbulator, whose geometry is depicted in Fig. 4. The height of the turbulator is of 3.3 mm and the resulting hydraulic diameter is equal to 2.5 mm according to the definition given by Manglik and Bergles [30].

The receiver coupled with the present asymmetrical parabolic trough concentrator consists of the illustrated absorber, which has been arranged on a support bar (Fig. 5) and thermally insulated on

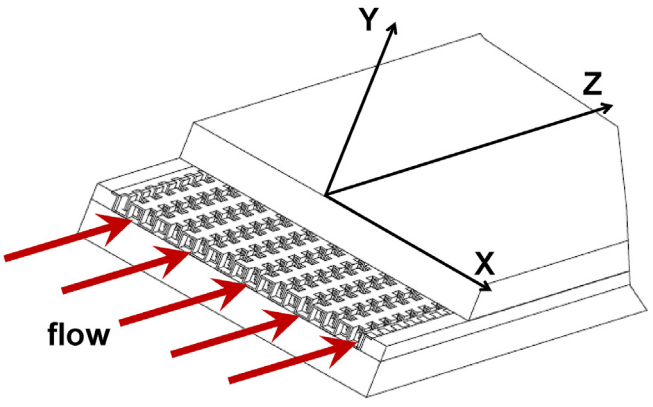

Fig. 4. Sketch of the offset strip turbulator geometry inside the flat receiver, including rectangular coordinates and flow direction.

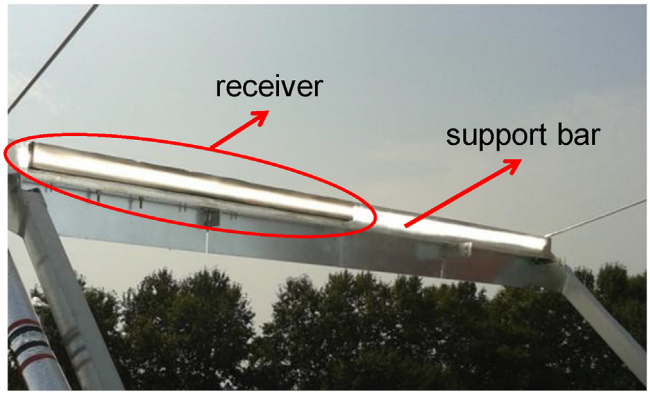

Fig. 5. Bar-and-plate flat receiver arranged on the support bar and illuminated with concentrated solar radiation during a test run.

the back side by using a 20 mm layer of rockwool. The front surface of the absorber is provided with a thickness insensitive spectrally selective black coating, that is characterized by a solar absorptance of around 90% and a thermal emittance at 100 °C of around 45%. The inlet and the outlet of the working fluid are located at the ends of the absorber on the back face. According to some preliminary tests, the maximum working pressure is 30 bar and the maximum working temperature is around 200 °C.

It is worth to mention that the bar-and-plate manufacturing process is extremely flexible. Thus, the dimensions of the absorber can be easily adapted in a cost-effective way to the primary optics of any considered medium temperature solar concentrating collector. As an example, in a symmetrical parabolic trough, a V-shaped absorber consisting of two flat parts could be easily realized.

2.2. Test rig

The test facility has been designed to measure the thermal efficiency of the solar concentrating collector during liquid heating but also when generating steam. In the latter case, the experimental investigation should validate of a test method compatible with the method available for liquid heating tests. Besides, possible instabilities during two phase flow must be carefully checked. Since the presence of a turbulator may penalize the hydraulic performance, accurate measurements of pressure drop have also to be carried out. The test rig includes a primary loop arranged on board the concentrating collector and a secondary cooling loop. Both the loops are thermally insulated to limit heat losses towards the surroundings. In the primary loop (Fig. 6), after exiting the receiver, the working fluid (distilled water) enters a tube-in-tube heat exchanger that acts as a heat sink: the heat transfer rate provided by the concentrated solar irradiance is taken away by a secondary water flow. In the heat sink, the distilled water flows inside the inner tube, while the coolant flows in the annulus. Afterwards, the distilled water is sent to an independently controlled gear pump magnetically coupled to a variable speed electric motor. This pump is used to set the mass flow rate, which is measured by a Coriolis effect mass flow meter. The pressure of the primary loop is regulated by a hydropneumatic accumulator with a fluoroelastomer diaphragm: this device plays an important role in direct steam generation test runs as the working pressure determines the temperature of the generated steam. Before entering the receiver, the fluid passes through a pre-heating section which consists of a heating wire wrapped around a stainless steel tube. The electrical heater is connected to a solid state relay which is governed by a PID temperature controller. The PID controller uses a T-type thermocouple as a probe to monitor the trend of the external wall temperature of the stainless steel pipe downstream of the pre-heating section. Three high precision absolute pressure sensors have been connected to the primary loop pressure taps to gauge the pressure at the inlet and at the outlet of the receiver and at the outlet of the tube-in-tube heat exchanger. The temperatures of the distilled water downstream of the pre-heating section, at the inlet and at the outlet of the receiver and downstream of the heat exchanger are measured by Pt100 resistance temperature detectors (RTDs). During the two phase tests for direct steam generation, with outlet vapor quality lower than 1, the presence of both the pressure transmitter and the RTD allows to check the agreement of temperature and pressure at the outlet of the receiver under saturated conditions. On the back of the receiver, under the thermal insulation layer, two flat RTDs have been attached to the aluminum wall at 300 mm from the inlet and at 300 mm from the outlet to measure the rear surface temperature of the bar-and-plate receiver. These measurements are useful to verify that the wall temperature never exhibits marked peaks, for example due to thermal dry out inside the receiver. The maximum operating temperature of the working fluid inside the primary loop during present tests is 140 °C.

In the secondary cooling loop (Fig. 6), the water coming from the tube-in-tube heat exchanger enters a storage and passes through a plate heat exchanger, where the heat gained from the primary loop is wasted to the ground water of the building central plant. Afterwards, the cooling water enters a second storage which is provided with four electrical heaters. Given the cooling mass flow rate, it is possible to set the electrical power in order to control the coolant temperature at the inlet of the tube-in-tube heat exchanger. A pump is used to circulate the coolant, whose mass flow rate is set by a control valve and is measured by a Coriolis effect mass flow meter. The controls on secondary mass flow rate and inlet temperature are useful to achieve constant conditions of the primary working fluid at the inlet of the receiver. The temperatures of the water at the inlet and at the outlet of the tube-in-tube heat exchanger are measured by Pt100 RTDs.

The laboratory is equipped with a measuring system of the solar irradiance including a first class pyrheliometer mounted on a high precision solar tracker that is used to measure the direct normal irradiance (DNI). Finally, an anemometer measures the wind speed on the horizontal plane and the ambient air temperature is gauged by a Pt100 RTD.

All the measured quantities are recorded by a data logger with sampling rate of 3 s and the collected data are reduced in a MATLAB environment by calculating the fluid properties with NIST Refprop Version 9.0 [31].

3. Experimental technique and data reduction

3.1. Single phase test runs

The thermal performance of the present parabolic trough linear solar concentrating collector, when working as a liquid heating device, has been evaluated according to the quasi-dynamic test method described in the European Standard EN ISO 9806:2013 [32]. This method was originally conceived for non concentrating solar collectors and for the relevant working temperature range and it was then extended to the concentrating technologies. As a consequence, when testing concentrating collectors, some procedures are hardly applicable [33] and some rules are unclear, especially for prototype testing.

According to this procedure, the specific mass flow rate is set equal to 0.02 kg s^{-1} per square meter of the aperture area, computed considering the actual length of the receiver (1.2 m) and the projected height of the mirrors. Measurements are repeated at

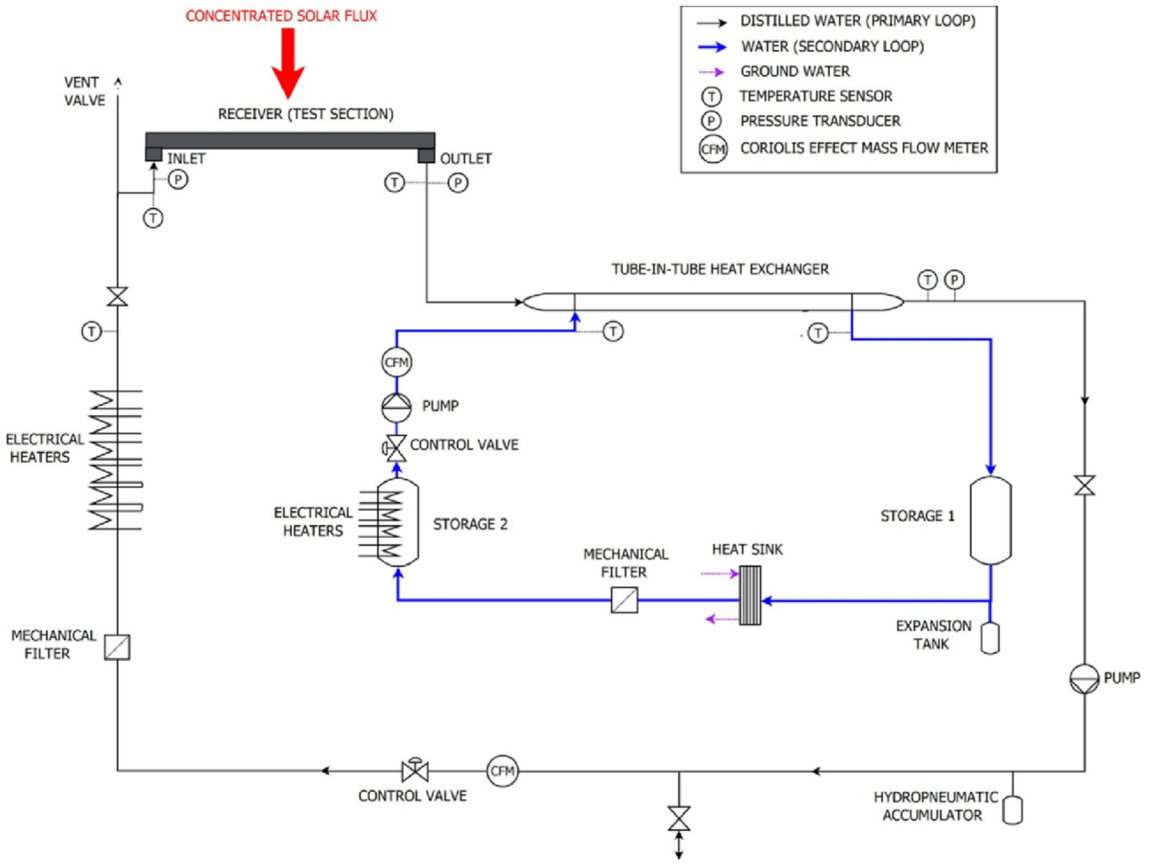

Fig. 6. Sketch of the experimental test rig.

different values of the inlet water temperature, in order to produce a set of data points for the thermal efficiency of the collector η_{th}, defined according to Eq. (2).

$$\eta_{th} = \frac{\dot{q}_{th}}{\mathrm{DNI}\, A_{ap}} = \frac{\dot{m}_I\, c_I \left(t_{out\ R,I} - t_{in\ R,I}\right)}{\mathrm{DNI}\, A_{ap}} \tag{2}$$

where c_I is the isobaric specific heat capacity of distilled water at the mean temperature between inlet and outlet of the receiver.

The experimental results are presented in a diagram plotting the experimental thermal efficiency as a function of the reduced temperature difference t_m^* (Eq. (3)), along with the obtained efficiency curve of the collector.

$$t_m^* = \frac{\frac{\left(t_{out\ R,I} + t_{in\ R,I}\right)}{2} - t_{amb}}{\mathrm{DNI}} = \frac{t_{m\ R,\ I} - t_{amb}}{\mathrm{DNI}} \tag{3}$$

The mathematical expression of the efficiency curve of the parabolic trough collector in quasi-dynamic conditions is defined in the standard. Its general equation is an energy balance including the dependence on direct and diffuse solar irradiance, wind speed, sky temperature, incidence angle effects and effective thermal capacity (Eq. (4)).

$$\begin{aligned}\frac{\dot{q}_{th}}{A_{ap}} = {} & \eta_{0,b} K_b G_b + \eta_{0,b} K_d G_d - c_6 u G - c_1 (t_m - t_{amb}) \\ & - c_2 (t_m - t_{amb})^2 - c_3 u (t_m - t_{amb}) + c_4 \left(E_L - \sigma_{SB} T_{amb}^4\right) \\ & - c_5 \frac{dt_m}{d\tau}\end{aligned} \tag{4}$$

In the present experimental study, concerning a concentrating system with two-axes sun tracker, the incidence angle modifier for direct radiation K_b is set equal to 1, the direct normal irradiance is used instead of the direct solar irradiance G_b and the incidence angle for diffuse radiation is equal to zero. In fact, the effective incident irradiance on the aperture area includes only the direct normal irradiance for all the concentrating collectors displaying a geometrical concentration ratio above 10 [34]. In the present work, the coefficients c_3, c_4 and c_6 are neglected right from the beginning, as it is recommended in the standard for concentrating collectors. Actually, according to the standard, it is not clear how the present concentrating collector prototype should be treated with respect to the effects of wind and long wave thermal irradiance. In fact, the case of an unglazed receiver installed in a device with a high concentration ratio is not contemplated. It is worth to mention that the test runs presented in this work have been performed in Padua, Italy (45.416° N, 11.883° E), where the wind speed in clear sky days is rarely higher than 1 m s^{-1}. Thus, the assumption of a negligible effect of wind is acceptable.

The experimental test rig does not include any storage and the working fluid temperature at the inlet of the receiver can be maintained within the limits imposed by the standard only by the

PID controlled electrical heaters and by varying the inlet temperature and the mass flow rate of the secondary fluid. As a consequence, the experimental tests have been conducted during clear sky days, when the variation of the direct normal irradiance is quite small. Thus the effect of the thermal capacity is not significant and is not included in the model ($c_5 = 0$). The final expression of the overall thermal efficiency is then:

$$\eta_{th} = \frac{\dot{q}_{th}}{\mathrm{DNI}\, A_{ap}} = \eta_0 - c_1 t_m^* - c_2 (t_m^*)^2\, \mathrm{DNI} \tag{5}$$

Eq. (5) can be further simplified when the coefficient c_2 is negative or has no statistical significance because the T-ratio, that is the ratio of the parameter value divided by its standard deviation, is lower than 3. As suggested by the standard EN ISO 9806:2013 [32], the weighted least square (WLS) method has been adopted to calculate the model parameters, starting from the measured quantities and their experimental uncertainties.

3.2. New test method for two phase test runs

The standard test methods to determine the thermal performance of solar concentrating collectors, namely the steady state method in the ASHRAE 93:2010 standard [35] and the quasi-dynamic method in EN 8609:2013 standard, refer to liquid or air heating devices. This means that the useful heat gained by the working fluid can be calculated considering its temperature increase inside the solar collector. There are no standard procedures to experimentally define the thermal efficiency of a solar concentrating collector performing direct steam generation, when a latent heat transfer is involved.

Few authors in the open literature [36,37] proposed different procedures for thermal performance evaluation of steam generating concentrating collectors. Bouvier et al. [37] pointed out that a proper definition of the reduced temperature difference should be introduced for two-phase systems. In this work, a new test procedure has been outlined to characterize the thermal performance of a solar collector in direct steam generation tests. It includes an expression for the reduced temperature difference in two-phase flow conditions that makes the data collected in direct steam generation consistent with those collected in liquid heating mode under standardized conditions.

During the test runs, the distilled water enters the test section as subcooled liquid and its thermodynamic condition is completely determined by the temperature and pressure measurements at the inlet of the receiver. The working fluid exits the receiver as saturated steam and then it is condensed and subcooled in the tube-in-tube heat exchanger. The thermodynamic state at the outlet of the heat sink is once again derived from pressure and temperature measurements. The tube-in-tube heat exchanger is installed very close to the outlet of the receiver, shielded from the concentrated solar beam and thermally insulated. The thermal balance in the tube-in-tube heat exchanger has been checked from the experimental points collected in single phase test runs and it results to be within ±3%. Given the above, the thermodynamic state of the working fluid at the outlet of the receiver under saturated conditions can be experimentally defined by applying the energy balance to the heat exchanger, under the reasonable hypothesis of negligible heat losses towards the surroundings. The specific enthalpy of the saturated steam at the outlet of the receiver can be expressed as reported in the following Eq. (6):

$$h_{out,R,I} = h_{out,HE,I}\left(t_{out,HE,I},\ p_{out,HE,I}\right) + \frac{\dot{m}_{II}\, c_{II}\left(t_{out,HE,\ II} - t_{in,HE,II}\right)}{\dot{m}_I} \tag{6}$$

where c_{II} is the isobaric specific heat capacity of the water flowing in the secondary loop at the mean temperature between the inlet and outlet of the tube-in-tube heat exchanger.

The thermodynamic vapor quality of the steam exiting the receiver can be obtained from Eq. (7), after calculating the saturated liquid specific enthalpy h_L and the heat of vaporization h_{LV} corresponding to the saturation temperature gauged at the outlet of the receiver:

$$x_{out,R,I} = \frac{h_{out,R,I} - h_L(t_{out,R,I})}{h_{LV}(t_{out,R,I})} \tag{7}$$

The saturation temperature is assumed equal to the temperature measured at the outlet of the receiver because, during steam generation test runs, the pressure drop across the receiver is very small: at 2 bar, for instance, the measured pressure drop entails a saturation temperature drop of 0.3 °C. Steam generation has been performed at different pressures of the distilled water inside the receiver and thus at different saturation temperatures in order to obtain a set of overall thermal efficiency data under two phase flow conditions, according to Eq. (8).

$$\eta_{th} = \frac{\dot{q}_{th}}{\mathrm{DNI}\, A_{ap}} = \frac{\dot{m}_I\ (h_{out\ R,I} - h_{in\ R,I})}{\mathrm{DNI}\, A_{ap}} \tag{8}$$

Considering Eq. (3), the definition of the reduced temperature difference under two phase flow requires the introduction of the equivalent mean temperature of the fluid during direct steam generation. Since the working fluid enters as subcooled liquid, both sensible and latent heat transfers occur inside the receiver of the solar concentrating collector. Hence, the equivalent mean temperature of the vaporizing working fluid shall be assumed as a weighted average temperature based on the enthalpy changes associated to the sensible and latent heat transfers (Eq. (9)).

$$t_{m\ eq,\ I} = \frac{\left(\frac{t_{out,R,I} + t_{in,R,I}}{2}\right)\left(h_L(t_{out,R,I}) - h_{in,R,I}\right) + t_{out,R,I}\left(h_{out,R,I} - h_L(t_{out,R,I})\right)}{h_{out,R,I} - h_{in,R,I}} \tag{9}$$

3.3. Experimental procedure

Before the test campaign, the primary loop is evacuated and filled with distilled water by using a centrifugal pump. The residual air content is removed by circulating the working fluid at high mass

flow rate while keeping the vent valve open. The vent valve is located near the receiver, on the highest part of the primary test loop. Prior to each test sequence, the mirrors and the sun sensor of the parabolic trough solar collector as well as the pyrheliometer have been cleaned.

When performing liquid heating tests, a preconditioning period of 20 min has been observed. During each test sequence, that has a minimum duration of 3 h, the experimental data are averaged every 10 min and the maximum permitted deviations of the main operating parameters are in agreement with the specifications included in the standard EN ISO 9806:2013 [32]. This means that each experimental point presented in this work is the average of 200 recordings while the collector is working under stable conditions.

During tests under steam generation (two phase flow regime), the new experimental procedure illustrated here below has been adopted. After a preconditioning period of 20 min, during each test sequence, that lasts for 3 h minimum, the collected data are averaged every 10 min and the following criteria have been satisfied during tests:

- the inlet temperature of subcooled liquid is kept stable within ±1 °C as compared to the mean value;
- the distilled water mass flow rate is kept stable within ±2% as compared to the mean value;
- the thermodynamic vapor quality at the outlet of the receiver must be higher than 0.1;

In order to validate this procedure, direct steam generation tests have been performed so that most of the useful heat (at least 90%) is transferred to the fluid flowing inside the receiver as latent heat. This entails that the maximum admitted subcooling degree for the data collected under two-phase flow regime is lower than 9 °C.

3.4. Experimental uncertainty analysis

The uncertainty analysis has been performed in agreement with the guidelines provided by the "Guide to the Expression of Uncertainty in Measurement" [38] and briefly recalled here below. The experimental standard uncertainty of a measured parameter is made up of two terms: the type A uncertainty that arises from the statistical analysis of repeated observations and the Type B uncertainty that results from calibration of instruments, calibration certificates, manufacturers' specifications and uncertainties assigned in reference handbooks. Type A uncertainty is the standard deviation of the mean and, in the present tests, it comes out considering 200 readings collected over the averaging time period of 10 min. Type B uncertainties of the measured parameters are reported in Table 1 with a level of confidence of 95%. Usually RTDs manufacturers provide a Type B uncertainty that depends on the measured temperature: for the present sensors it is ±0.04 °C at 5 °C and ±0.1 °C at 90 °C. In Table 1, the type B uncertainty of the RTDs is reported as a constant value of ±0.035 °C, which is valid within the temperature test range from 20 °C to 150 °C. This value results from the calibration procedure performed using a high precision four wire RTD, that is calibrated up to 150 °C. The reference RTD is connected to a Hart Scientific Super Thermometer II providing a measure chain with a global accuracy within ±0.01 °C. In order to calibrate the RTDs, a copper cylinder with a diameter of 60 mm and a height of 150 mm is employed. Several 100 mm deep holes have been manufactured on the top face of the cylinder to accommodate the temperature sensors. During calibration, all the RTD sensors and the copper cylinder are arranged inside a laboratory oven where the temperature set point can be varied. A correction function for each RTD is defined by comparing the temperatures measured by each RTD against the reference temperatures within the calibration range.

With respect to the parameters which are not directly measured, their combined standard uncertainty can be calculated by applying the law of error propagation. For a given parameter, the expanded experimental uncertainty is obtained by multiplying the relevant standard uncertainty by a coverage factor equal to 2, which corresponds to a level of confidence of 95%. Finally, the uncertainties of the coefficients in the function of the efficiency curve result from the use of the weighted least square (WLS) method, which is described in details in the standard EN ISO 9806:2013 [32]. This method can be extended to the data collected during direct steam generation, considering the relevant parameters defined in Section 3.2.

4. Results and discussion

The experimental tests have been performed in clear sky days in Padua, Italy (45° 24′ 23″ N, 11° 52′ 40″ E) from October to June.

Six test sequences with the parabolic trough working as a liquid heating solar collector have been carried out and 91 data points have been collected. The direct normal irradiance was between 500 W m^{-2} and 860 W m^{-2}, the ambient air temperature between 8 °C and 33 °C, the mass flow rate of the distilled water in the primary loop was set equal to 0.02 kg s^{-1} per square meter of the aperture area, which corresponds to a total mass flow rate of 250 kg h^{-1}. The temperature of the distilled water at the inlet of the receiver has been set at 37 °C, 48 °C, 50 °C, 81 °C, 109 °C and 117 °C to obtain experimental data in the reduced temperature difference range between 0.025 K m^2 W^{-1} and 0.140 K m^2 W^{-1}.

The experimental campaign performing steam generation consists of four test sequences, during which 26 experimental points have been collected at saturation temperature of 120 °C, 123 °C, 131 °C and 138 °C. Considering the collected data, averaged every 10 min, the deviation between the measured temperature and the saturation temperature calculated from the pressure at the outlet of the receiver is within ±0.05 °C, that is within the experimental uncertainty of the two employed instruments. During the steam generation tests, the subcooling at the inlet of the receiver was between 6 °C and 9 °C and the mass flow rate between 11 kg h^{-1} and 12.5 kg h^{-1} with a thermodynamic vapor quality at the outlet of the receiver between 0.2 and 0.3. These values are due to the small length of the tested receiver and to the minimum mass flow rate that can be pumped in the primary loop. Higher vapor qualities can

Table 1
Type B uncertainty of measured parameters.

Ambient air temperature	±0.07 °C
Fluid temperature in primary and secondary loops	±0.035 °C
Coriolis effect mass flow meters	±0.3 kg h^{-1} for single phase tests ±0.07 kg h^{-1} for two phase tests
Pressure of the fluid in the primary loop	±0.023 bar
Direct normal irradiance	±3% of measured value
Wind speed	± (0.1 m/s + 1% of measured value)

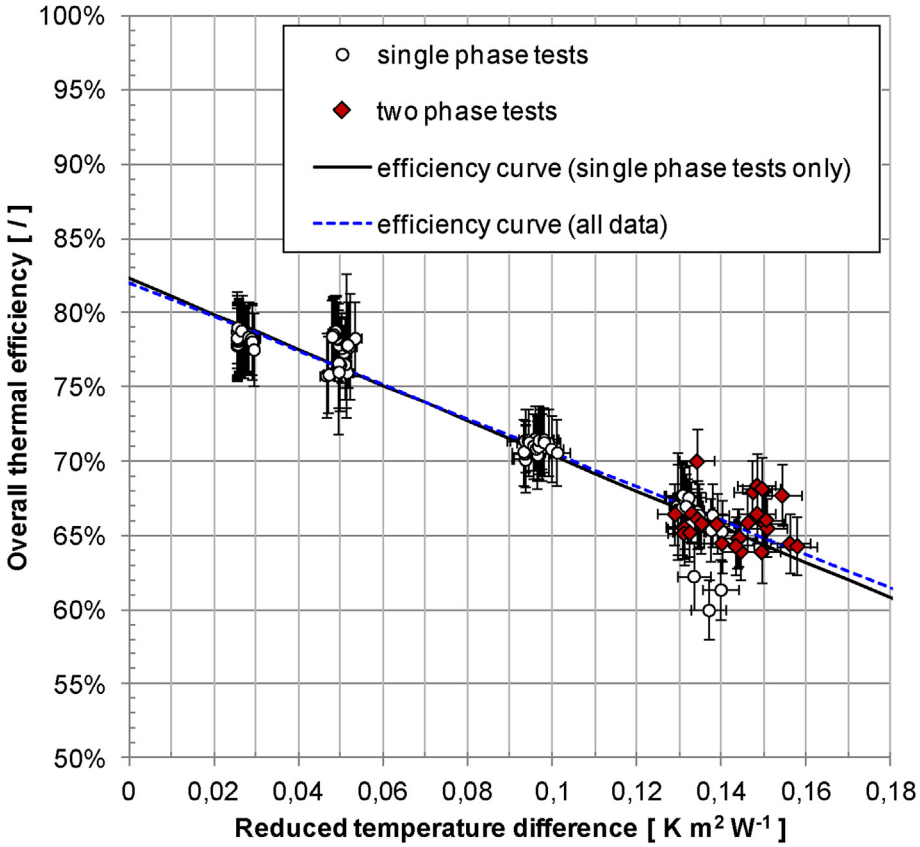

Fig. 7. Experimental thermal efficiency of the present parabolic trough collector data versus reduced temperature difference. The efficiency curves reported in the graph are derived considering only single phase tests and then considering all the collected data.

Table 2
Parameters of the parabolic trough collector's efficiency curve calculated according to the guidelines of the quasi-dynamic test method illustrated in the standard EN ISO 9806:2013.

Parameter	Only liquid heating tests		Complete database (liquid heating + direct steam generation tests)	
	Value	Expanded uncertainty	Value	Expanded uncertainty
η_0	0.8230	0.0055	0.8203	0.0051
c_1	−1.1951	0.0649	−1.1455	0.0501

be achieved in a longer receiver. The direct normal irradiance was between 650 W m^{-2} and 860 W m^{-2} and the ambient air temperature between 15 °C and 23 °C. In these two phase tests, the range of the reduced temperature difference, calculated as reported in section 3.2, varies from 0.130 K m^2 W^{-1} to 0.160 K m^2 W^{-1}.

All the collected experimental points are plotted with the corresponding error bands in Fig. 7 along with two efficiency curves expressed in the mathematical form of Eq. (5). The expanded experimental uncertainty on the thermal efficiency ranges between ±1.9% and ±3.1% while the maximum expanded experimental uncertainty on the reduced temperature difference is of ±0.005 K m^2 W^{-1}. The coefficients calculated according to the weighted least square (WLS) method are reported in Table 2, with the relevant expanded standard uncertainties (level of confidence 95%). The solid line represents the efficiency curve defined using only the experimental data collected in liquid heating mode, according to the guideline of the quasi-dynamic test method. The dashed line is the efficiency curve obtained considering all the data, i.e. the test runs both in liquid heating working mode and in direct steam generation. From Table 2, it can be seen that both efficiency curves are straight lines: in fact, from the data reduction, the T-ratio of the coefficient c_2 is always smaller than 3, so c_2 has no statistical significance. Hence, the parameter identification has been repeated without c_2 included in the model. From Fig. 7, one can observe that there is a very good agreement between the two efficiency curves and that the experimental data measured during liquid heating and during steam generation overlap at reduced temperature differences between 0.130 K m^2 W^{-1} and 0.140 K m^2 W^{-1}. This means that the present new procedure proposed for data reduction during two phase test runs gives results consistent with those derived from the standardized procedure. Therefore, it can be adopted to characterize the thermal performance of a solar concentrating collector. In particular, controlling the inlet subcooling degree, one can reach an equivalent mean temperature of the fluid inside the receiver as close as possible to the maximum operating temperature for a given saturation pressure.

Since the efficiency curve derived from the whole database displays a lower uncertainty of the overall thermal efficiency, the following discussion refers to that curve. The experimental optical efficiency comes out to be equal to 82%. This value is partly due to

the high reflectivity of the back silvered glass facets forming the primary optics but it also indicates that the coupling of the parabolic trough mirror with a flat geometry absorber may be an interesting option for medium temperature applications. The thermal efficiency of the present parabolic trough collector at 0.16 K m^2 W^{-1} is equal to 64% that is remarkable as compared to some medium temperature concentrating collectors available on the market and can still be improved. In fact, in the tested prototype, the receiver consists only of a flat absorber provided with a black coating so it is not optimized for the minimization of the thermal losses. Higher efficiency may be achieved by arranging this absorber as a part of a cavity receiver provided with a front clear borosilicate glass. Furthermore, on the front surface of the absorber, a selective coating with a lower emittance in the infrared region might be employed.

The hydraulic performance of the proposed receiver can be assessed by considering the difference between the measured pressures at the inlet and at the outlet of the receiver. During tests in liquid heating mode, the pressure drop across the receiver is within 0.10 bar–0.13 bar, while during direct steam generation test runs it is around 0.02 bar, that is within the experimental uncertainty of the pressure transducers. Hence, the bar-and-plate absorber is particularly suitable for direct steam generation, since the presence of the turbulator for heat transfer enhancement leads to pretty low additional pressure drop. On the other hand, the geometry of the turbulator should be optimized for the application in single phase flow regime.

In direct steam generation, the difference between the temperatures on the back surface of the absorber, measured by the flat RTDs, and the saturation temperature is always lower than 1 K. This proves that the vaporization process can be performed at mass flow rates down to 11 kg h^{-1} without originating any hot spot or instability due to dry out of the liquid film at the wall.

Finally, the time constant of the collector has been calculated following the procedure reported in the standard EN ISO 9806:2013 [32]. At first, the concentrator is manually defocused so that no concentrated radiation reaches the receiver and the fluid inlet temperature is set close to the ambient air temperature. During this test, the electrical heaters of the preheating were switched off and the circulating mass flow rate was set equal to 250 kg h^{-1},which is the value used during liquid heating tests. The direct normal irradiance was around 830 W m^{-2}. Once reached a steady-state condition, the tracking system of the collector is switched on to focus the solar beams on the absorber within few seconds. Readings continue until the steady state conditions are reached again, which means that the outlet temperature of the fluid varies less than 0.5 °C per minute. The difference between outlet fluid temperature and ambient air temperature is plotted against time in Fig. 8. The collector time constant can be calculated as the elapsed time between the focusing of the concentrator on the absorber and the time when the difference between the outlet fluid temperature and the ambient air temperature rises to 63.2% of the total increase from the starting to the final value. The time constant of the present asymmetrical parabolic trough solar collector results equal to 213 s, thus the collector stabilizes quickly. The preconditioning period of 20 min adopted during test runs is long enough to ensure that the initial conditions of the system does not affect the experimental results.

5. Conclusions

A prototype of medium temperature solar concentrating

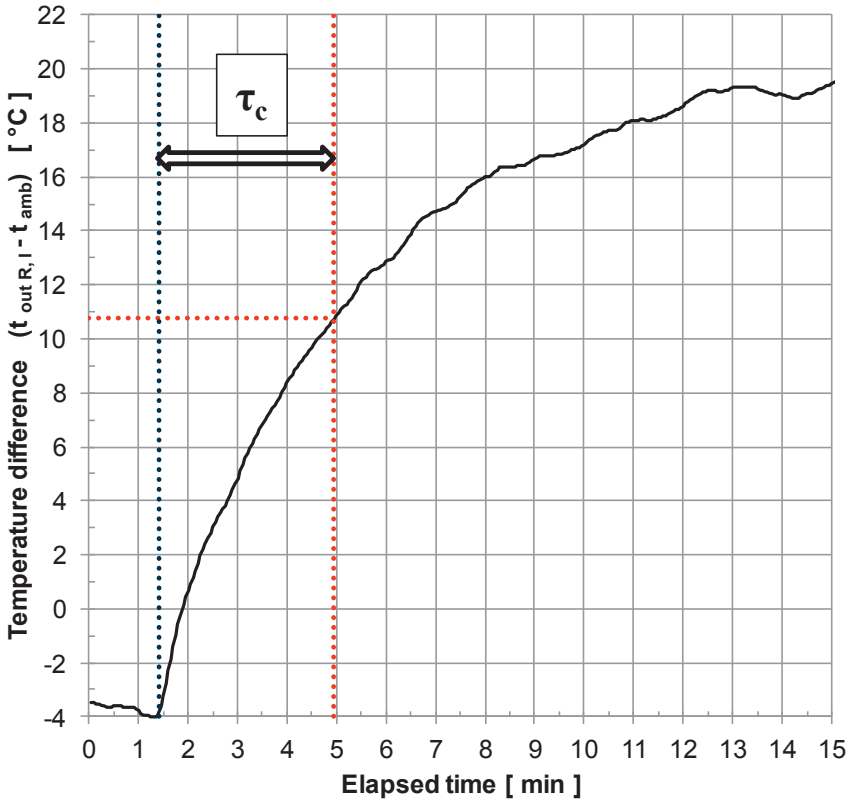

Fig. 8. Time constant τ_c of the present asymmetrical parabolic trough solar collector according to the standard EN ISO 9806:2013.

collector, made of an asymmetrical parabolic trough concentrator and an innovative bar-and-plate flat aluminum absorber, has been tested during both liquid heating and direct steam generation. For the latter test mode, a new procedure has been proposed, including the definition of reduced temperature difference in two-phase flow conditions. The results show that:

1 The two efficiency curves derived considering only the single phase tests or the whole collected database in single phase and two phase tests are in very good agreement. Furthermore, the single and two phase flow datasets overlap at reduced temperature differences between 0.130 K m^2 W^{-1} and 0.140 K m^2 W^{-1}. Therefore, the present new test procedure proposed for direct steam generation tests is validated and can be adopted to characterize the thermal performance of a concentrating collector.
2 The experimental optical efficiency of the present prototype is equal to 82%, while the thermal efficiency at 0.160 K m^2 W^{-1} is around 64%, which is a promising value and can still be improved by arranging the flat absorber as a part of a cavity receiver and by adopting a solar selective coating with a low thermal emittance. The time constant of the collector is equal to 213 s.
3 Regarding the hydraulic performance, despite the presence of the turbulator in the channel, low pressure drop during direct steam generation have been measured. Moreover, the measured temperature of the absorber back surface is close to the saturation temperature of the vaporizing fluid without any hot spot associated with thermal dry out. This demonstrates that the present bar-and-plate absorber is suitable for direct steam generation even at low mass flow rates.

Acknowledgements

The support of Nardini Consulting for the fabrication and provision of the bar-and-plate absorber is greatly acknowledged.

References

[1] International Energy Agency. Key world energy statistics. Paris, France. 2015.
[2] European Solar Thermal Industry Federation. Solar industrial process heat - state-of-the-art. 2006. within Task 3.5 of Key Issues for Renewable Heat in Europe (K4RES-H) project.
[3] Vannoni C, Battisti R, Drigo S. Potential for solar heat in industrial processes. IEA SHC task 33 and SolarPACES task IV Gleisdorf AEE INTEC. 2008.
[4] Cabrera FJ, Fernández-García A, Silva RMP, Pérez-García M. Use of parabolic trough solar collectors for solar refrigeration and air-conditioning applications. Renew Sustain Energy Rev 2013;20:103–18.
[5] Fernández-García A, Zarza E, Valenzuela L, Pérez M. Parabolic-trough solar collectors and their applications. Renew Sustain Energy Rev 2010;14:1695–721.
[6] Zarza E. Medium temperature solar concentrators (parabolic trough collectors). In: Galvez J, Malato Rodriguez S, editors. Solar energy conversion and photoenergy systems, vol. 1. Paris: EOLSS Publishers; 2009. p. 170.
[7] Zhu G, Wendelin T, Wagner MJ, Kutscher C. History, current state, and future of linear Fresnel concentrating solar collectors. Sol Energy 2014;103:639–52.
[8] Montes MJ, Rubbia C, Abbas R, Martínez-Val JM. A comparative analysis of configurations of linear Fresnel collectors for concentrating solar power. Energy 2014;73:192–203.
[9] Pye J, Morrison G, Behnia M. Transient modelling of cavity receiver heat transfer for compact linear Fresnel reflector. In: Proceedings of ANZSES 2003 destination renewable conference, Melbourne, Australia; 2003.
[10] Reynolds DJ, Jance MJ, Behnia M, Morrison GL. An experimental and computational study of the heat loss characteristics of a trapezoidal cavity absorber. Sol Energy 2004;76:229–34.
[11] Khanna S, Kedare SB, Singh S. Analytical expression for circumferential and axial distribution of absorbed flux on a bent absorber tube of solar parabolic trough concentrator. Sol Energy 2013;92:26–40.
[12] Eck M, Uhlig R, Mertins M, Häberle A, Lerchenmüller H. Thermal load of direct steam-generating Absorber tubes with large diameter in horizontal linear Fresnel collectors. Heat Transf Eng 2007;28:42–8.
[13] Wang P, Liu DY, Xu C. Numerical study of heat transfer enhancement in the receiver tube of direct steam generation with parabolic trough by inserting metal foams. Appl Energy 2013;102:449–60.
[14] Khanna S, Kedare SB, Singh S. Deflection and stresses in absorber tube of solar parabolic trough due to circumferential and axial flux variations on absorber tube supported at multiple points. Sol Energy 2014;99:134–51.
[15] Khanna S, Singh S, Kedare SB. Explicit expressions for temperature distribution and deflection in absorber tube of solar parabolic trough concentrator. Sol Energy 2015;114:289–302.
[16] Muñoz J, Abánades A. Analysis of internal helically finned tubes for parabolic trough design by CFD tools. Appl Energy 2011;88:4139–49.
[17] Cheng ZD, He YL, Cui FQ. Numerical study of heat transfer enhancement by unilateral longitudinal vortex generators inside parabolic trough solar receivers. Int J Heat Mass Transf 2012;55:5631–41.
[18] Ghadirijafarbeigloo S, Zamzamian AH, Yaghoubi M. 3-D numerical simulation of heat transfer and turbulent flow in a receiver tube of solar parabolic trough concentrator with louvered twisted-tape inserts. Energy Procedia 2014;49:373–80.
[19] Song X, Dong G, Gao F, Diao X, Zheng L, Zhou F. A numerical study of parabolic trough receiver with nonuniform heat flux and helical screw-tape inserts. Energy 2014;77:771–82.
[20] Mwesigye A, Bello-Ochende T, Meyer JP. Heat transfer and thermodynamic performance of a parabolic trough receiver with centrally placed perforated plate inserts. Appl Energy 2014;136:989–1003.
[21] Mwesigye A, Bello-Ochende T, Meyer JP. Multi-objective and thermodynamic optimisation of a parabolic trough receiver with perforated plate inserts. Appl Therm Eng 2015;77:42–56.
[22] Reddy KS, Ravi Kumar K, Ajay CS. Experimental investigation of porous disc enhanced receiver for solar parabolic trough collector. Renew Energy 2015;77:308–19.
[23] Rojas ME, de Andrés MC, González L. Designing capillary systems to enhance heat transfer in LS3 parabolic trough collectors for direct steam generation (DSG). Sol Energy 2008;82:53–60.
[24] Almanza R, Jiménez G, Lentz A, Valdés A, Soria A. DSG under two-phase and stratified flow in a steel receiver of a parabolic trough collector. J Sol Energy Eng 2002;124:140–4.
[25] Almanza R, Lentz A, Jiménez G. Receiver behavior in direct steam generation with parabolic troughs. Sol Energy 1997;61:275–8.
[26] Flores V, Almanza R. Direct steam generation in parabolic trough concentrators with bimetallic receivers. Energy 2004;29:645–51.
[27] Aldali Y, Muneer T, Henderson D. Solar absorber tube analysis: thermal simulation using CFD. Int J Low Carbon Technol 2013;8:14–9.
[28] National Renewable Energy Laboratory. SolTrace version 2012.7.9. 2012.
[29] Neumann A, Witzke A, Jones SA, Schmitt G. Representative terrestrial solar brightness profiles. J Sol Energy Eng 2002;124:198–204.
[30] Manglik RM, Bergles AE. Heat transfer and pressure drop correlations for the rectangular offset strip fin compact heat exchanger. Exp Therm Fluid Sci 1995;10:171–80.
[31] Lemmon EW, Huber ML, McLinden MO. NIST standard Reference Database 23: reference fluid thermodynamic and transport properties - REFPROP. 9.0. 2010.
[32] Comitè Europeen de Normalisation (CEN). Solar energy - solar thermal collectors - test methods (ISO 9806:2013). 2013.
[33] Xu L, Wang Z, Li X, Yuan G, Sun F, Lei D, et al. A comparison of three test methods for determining the thermal performance of parabolic trough solar collectors. Sol Energy 2014;99:11–27.
[34] Duffie JA, Beckman WA. In: Hoboken, editor. Solar engineering of thermal processes. fourth ed. New Jersey, U.S.A.: John Wiley & Sons Inc; 2014.
[35] ANSI/ASHRAE Standard 93-2010 (RA 2014). Methods of testing to determine the thermal performance of solar collectors. 2014.
[36] Sardeshpande VR, Chandak AG, Pillai IR. Procedure for thermal performance evaluation of steam generating point-focus solar concentrators. Sol Energy 2011;85:1390–8.
[37] Bouvier J, Michaux G, Salagnac P, Nepveu F, Rochier D, Kientz T. Experimental characterisation of a solar parabolic trough collector used in a micro-CHP (micro-cogeneration) system with direct steam generation. Energy 2015;83:474–85.
[38] Joint Committee for Guides in Metrology. Evaluation of measurement data — Guide to the expression of uncertainty in measurement (JCGM 100:2008). 2008.